

Global Self-Attention with Exact Fourier Propagation for Phase-Only Far-Field Holography

Dilawer Singh^{1*}, Antoni J. Wojcik¹ and Timothy D. Wilkinson¹

¹Electrical Engineering, University of Cambridge, 9 JJ Thomson Ave, Cambridge, CB3 0FA, England.

*Corresponding author(s). E-mail(s): ds2070@cam.ac.uk;
Contributing authors: ajw308@cam.ac.uk; tdw13@cam.ac.uk;

Abstract

Phase-only computer-generated holography (CGH) seeks a phase pattern for a spatial light modulator (SLM) whose propagated optical field reproduces a desired intensity distribution. In the far-field (Fraunhofer) regime, optical propagation reduces to a Fourier transform, such that each hologram pixel contributes to the entire reconstructed intensity distribution. When restricted to phase-only modulation, intensity must be shaped through global phase interference effects, making the inverse mapping from target intensity to phase highly non-linear and sensitive to local minima. We present a proof-of-concept physics-in-the-loop approach in which a transformer maps a target intensity image to a phase-only SLM field and is trained end-to-end through exact FFT-based propagation embedded directly within optimization. We further observe that patch tokenization strongly shapes the optimization geometry: coarse tokenization acts as an implicit spectral regularizer that stabilizes training and suppresses checkerboard-like attractors, while finer tokenization increases spatial degrees of freedom but benefits from curriculum or hierarchical refinement. Despite training on limited primitives and restricted digit subsets, the learned generator exhibits out-of-distribution (OOD) generalization to unseen digits and hand-drawn target patterns. These results suggest that transformer architectures, whose self-attention enables global token interactions, are a natural fit for far-field holography and provide a viable foundation for scalable physics-grounded hologram generation.

Keywords: Fraunhofer Diffraction, Computer-Generated Holography, Transformer, Self-Attention, Deep Learning

1 Introduction

Computer-generated holography (CGH) seeks to determine a phase pattern $\phi(x, y)$ displayed on a spatial light modulator (SLM) such that, after optical propagation, the resulting intensity distribution matches a desired target. In the far-field (Fraunhofer) regime, scalar diffraction theory shows that propagation reduces to a Fourier transform. [1] Let the complex field immediately after the SLM be

$$U_0(x, y) = e^{j\phi(x, y)}, \quad (1)$$

where the amplitude is fixed to unit magnitude and only the phase is modulated.

Under far-field propagation, the complex field in the reconstruction plane is given by

$$U_f(u, v) = \mathcal{F}\{U_0(x, y)\}, \quad (2)$$

and the observed intensity is

$$I_f(u, v) = |U_f(u, v)|^2. \quad (3)$$

The inverse problem is therefore: given a desired target intensity $I^T(u, v)$, find a phase distribution $\phi(x, y)$ such that

$$I_f(u, v) \approx I^T(u, v).$$

Two structural properties make this problem challenging. First, the Fourier transform is a global operator, meaning each SLM pixel contributes to the entire far-field distribution. Consequently, local phase adjustments influence global intensity patterns. Second, because the SLM modulates phase only, intensity must be shaped through phase interference rather than in conjunction with amplitude control, resulting in a highly non-linear mapping from ϕ to I_f .

This problem has traditionally been addressed using alternating-projection methods. The Gerchberg–Saxton (GS) algorithm iteratively enforces intensity constraints in both planes while keeping phase the degree of freedom (DOF). [2] Hybrid input–output variants and related improvements to mitigate stagnation and accelerate convergence were later introduced. [3] These methods remain foundational, but require multiple iterations per target and may converge to local minima depending on initialization and constraint choices, yielding sub-optimal reconstructions.

Recent advances in deep learning have motivated hologram generation, where a neural network predicts a hologram in a single forward pass. Early work demonstrated neural networks for phase recovery and holographic reconstruction. [4] Subsequent reviews summarize rapid progress in deep-learning-based CGH, including convolutional neural networks trained to generate holograms directly and camera-in-the-loop frameworks that learn propagation corrections jointly with hardware calibration. [5–8]

Most of this work operates in Fresnel or near-field regimes, frequently modeled using the angular spectrum method (ASM). For example, recent attention-enhanced convolutional approaches have been proposed for ASM-based hologram generation. [9] In contrast to Fresnel or ASM formulations, where propagation can retain partially

local structure depending on sampling and depth, the Fraunhofer regime reduces to Fourier propagation, eliminating spatial locality in the forward operator. Neural networks have also been applied to complex hologram representations for recognition tasks.[10] But, these approaches process holographic data as input, rather than synthesizing phase-only holograms under explicit propagation constraints.

The structural properties of far-field propagation therefore have direct consequences for model design. Generating a valid phase-only solution requires coordinated structure across distant regions of the phase field, reflecting the nonlocal coupling inherent to far-field diffraction. This observation suggests that architectural inductive biases capable of modeling long-range interactions may be particularly well suited to far-field hologram synthesis.

Classical convolutional neural networks, originally popularized for image recognition, emphasize locality through finite receptive fields and weight sharing.[11] Although deep networks can approximate global interactions, their architectural prior emphasizes locality, which is highly effective for natural images but may be less directly aligned with nonlocal diffraction operators.

Transformers, however, introduced by Vaswani et al., implement global token interactions through self-attention.[12] In scaled dot-product attention, each token aggregates information from every other token in a single layer, allowing the model to represent global dependencies explicitly.

When applied to images, Vision Transformers (ViT) demonstrated that spatial patches can be treated as tokens and processed through global attention mechanisms.[13] Patch tokenization not only restructures the image into interaction units but also controls the effective spatial degrees of freedom available to the model.

In far-field holography, Fourier propagation mixes spatial information across the reconstruction plane, and such interaction mechanisms provide a structurally aligned inductive bias. This alignment between architectural bias and physical structure motivates the investigation of transformer-based models for phase-only far-field hologram generation under explicit physics-in-the-loop training. An additional practical advantage of this formulation is inference speed. Once trained, the network generates a phase hologram in a single forward pass, eliminating iterative per-target optimization required by alternating-projection methods such as Gerchberg–Saxton. This enables effectively constant-time hologram synthesis at inference.

2 Methods

2.1 Physics-in-the-Loop Far-Field Generation

In this work, we consider a phase-only far-field hologram generator \mathcal{G} trained end-to-end with exact FFT-based propagation in the loop:

$$I^T \longrightarrow \mathcal{G} \longrightarrow e^{j\hat{\phi}(x,y)} \longrightarrow \mathcal{F} \longrightarrow I_f \longrightarrow \mathcal{L}(I_f, I^T).$$

where \mathcal{G} is an attention-based generator parameterized by global self-attention layers, and \mathcal{L} is the loss between the predicted far-field intensity, I_f , and the target intensity, I^T .

Rather than learning a surrogate model of optical propagation, we embed the Fourier operator directly within the computational pipeline during training. The model outputs the complex field $e^{j\hat{\phi}(x,y)}$ which is propagated via a discrete Fourier transform implemented as an FFT. Intensity formation is computed explicitly as the squared magnitude of the propagated field. Thus, the forward pass consists of

$$U_0 = e^{j\hat{\phi}}, \quad (4)$$

$$U_f = \mathcal{F}\{U_0\}, \quad (5)$$

$$I_f = |U_f|^2. \quad (6)$$

The complete optical model is differentiable, with gradients propagated through both the intensity operation and Fourier transform using complex-valued automatic differentiation. No learned approximation of the propagation operator is introduced. The phase-only constraint is enforced directly through the unit-modulus $U_0 = e^{j\hat{\phi}}$, ensuring that optimization occurs over the physically-relevant phase manifold.

2.2 Attention-Based Phase Generator

To approximate the inverse mapping $I^T \mapsto \phi$, we employ a transformer-based generator \mathcal{G} that maps a target intensity image to a phase field of matching spatial resolution. For the 28×28 experiments, the input is partitioned into a coarse 2×2 grid of non-overlapping patches (patch size 14, $T = 4$ tokens). Each patch is flattened and linearly embedded into a latent vector ($d = 256$), and a 2D sinusoidal positional encoding is added to retain spatial layout. The resulting token sequence is processed by a multi-layer transformer encoder (stacked multi-head self-attention and feed-forward blocks) to model the global, nonlocal coupling induced by Fourier propagation. A final projection maps the encoded tokens back to a 28×28 phase map (implemented as a unit-modulus complex field as described in Section 2.1). The resulting model contains 3,306,120 trainable parameters.

Patch tokenization controls the effective spatial degrees of freedom available to the model. Coarser tokenization constrains high-frequency phase variation and acts as an implicit regularizer, whereas finer tokenization increases representational capacity. Specific architectural hyperparameters and certain optimization details are intentionally omitted in this preprint and will be provided in subsequent full publications.

2.3 Loss Function and Energy Scaling

Training is performed in the intensity domain using an energy-scaled mean squared error (MSE) loss. Let \tilde{I}^T denote a normalized version of the target intensity. We rescale the normalized target so that its total energy matches that of the predicted field:

$$I_E^T = \tilde{I}^T \cdot (HW), \quad (7)$$

where H and W denote height and width, respectively. Training minimizes the energy-scaled MSE between the reconstructed intensity, I_f , and the rescaled target intensity, I_E^T , where the subscript E denotes normalization to matched total optical energy between prediction and target. The loss function is defined as

$$\mathcal{L} = \frac{1}{HW} \|I_f - I_E^T\|^2. \quad (8)$$

This formulation enforces agreement in physical intensity space while maintaining consistent energy scaling across training samples.

2.4 Experimental Overview

We evaluate physics-in-the-loop transformer training for phase-only far-field hologram synthesis on 28×28 target intensity patterns. The goal is to predict a phase-only hologram whose propagated far-field intensity matches a desired target. Performance is assessed using Equation 8.

All experiments use the exact FFT-based Fraunhofer forward model described in Section 2.1. Unless stated otherwise, all reported metrics are computed on held-out validation and test splits defined within the same experimental pipeline. The final results correspond to the last stage of curriculum training, with each stage initialized from the previous checkpoint. Curriculum training is defined here as staged optimization beginning with structured spatial-frequency primitives and progressively introducing more complex targets.

2.5 Training Data and Curriculum

To encourage broad generalization beyond any single dataset, we train on a mixed synthetic + real-intensity curriculum that incrementally increases target complexity. The final stage training set aggregates multiple categories including procedurally generated patterns (e.g., structured basis-like stimuli, symmetric dot patterns, sparse and dense random patterns, and gratings), as well as large sets of synthetic shapes, doodles, and band-limited smooth textures. Additionally, digit-like and apparel-like targets are included via MNIST and Fashion-MNIST samples.[14][15] In the final stage, the training set composition is presented in Table 1.

Across stages, each new curriculum tier is trained by loading the previous tier’s model weights and continuing optimization. This staged procedure is intended to stabilize learning of the physically constrained inverse mapping by first mastering simpler spatial-frequency primitives before progressing to natural-image-like targets.

2.6 Optimization and Hyperparameters

The final training stage uses batch size $B = 64$ for 1000 epochs. The learning rate is initialized at 5×10^{-3} and decayed multiplicatively every 100 epochs (effective learning rate at the end of training is $\approx 3.15 \times 10^{-3}$). The best model is selected by minimum validation loss and then evaluated on the test split.

Table 1: Final-stage training dataset composition.

Dataset Component	Number of Samples
Synthetic shapes	4000
Doodles	3000
Smooth band-limited textures	2000
Single-pixel basis patterns	50
Symmetric dot patterns	50
Sparse random patterns	50
Dense random patterns	50
Grating patterns	32
MNIST digits	3000
Fashion-MNIST images	3000
Total	15,232

3 Results

3.1 Quantitative Results

Table 2: Final quantitative performance (MSE).

Metric	MSE
Training MSE	0.6304
Validation MSE	0.6411
Test MSE	0.6614

For the final stage run, the model achieves the following results presented in Table 2. These values indicate stable convergence under physics-in-the-loop optimization and consistent generalization from training to held-out data within the same evaluation protocol.

To probe OOD behavior on digit targets, we additionally sample $n = 10$ examples per digit from the full MNIST test set (digits 0–9) and report mean MSE per digit. Despite training that included a digit-restricted curriculum tier (and later broad synthetic targets), the trained model produces recognizable far-field digit structure across all classes. The per-digit OOD mean MSE is presented in Table 3. We observe the lowest OOD error on digit 6 in this sampled evaluation, consistent with the curriculum including a digit-specific tier.

3.2 Qualitative Results

Figure 1 shows one representative OOD example per digit (top row: target intensity; bottom row: model-predicted far-field intensity). The reconstructions preserve

Table 3: OOD MNIST digit performance (mean MSE, $n = 10$ per digit).

Digit	Mean MSE
0	0.9892
1	2.0946
2	1.1272
3	1.2964
4	1.1281
5	1.3749
6	0.8256
7	1.7004
8	1.0858
9	1.0337

digit identity with noticeable speckle-like artifacts, reflecting the difficulty of satisfying phase-only constraints while matching fine-grained target intensities. Figure 2 shows the training MSE trajectory over 1000 epochs, demonstrating rapid initial descent followed by gradual improvement.

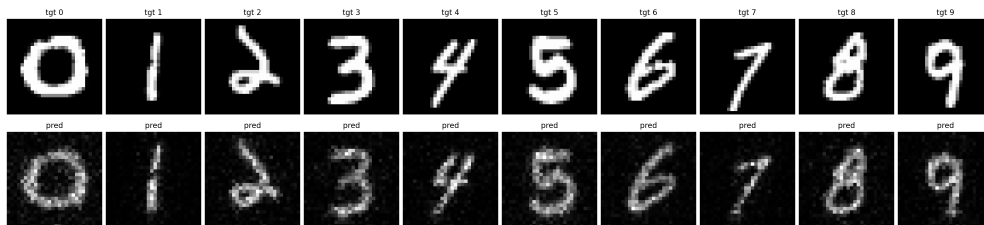


Fig. 1: OOD MNIST digits: one example per class. Top: target intensity. Bottom: predicted far-field intensity obtained from the phase-only hologram produced by the model and propagated via FFT-based Fraunhofer diffraction.

3.3 Generalization to Custom Hand-Drawn Targets

To evaluate generalization beyond procedurally generated patterns and standard benchmarks, we tested the trained model on four manually constructed 28×28 grayscale targets not drawn from MNIST, Fashion-MNIST, or any synthetic generator used during training. These targets contain irregular composite structures and spatial configurations distinct from the training distribution.

Figure 3 shows, for each example, the predicted phase hologram, the corresponding reconstructed far-field intensity, and the target intensity. The resulting MSE values are reported in Table 4.

Despite the strict phase-only constraint and extremely low spatial resolution, the reconstructions preserve the dominant geometric structure of the targets. At 28×28 ,

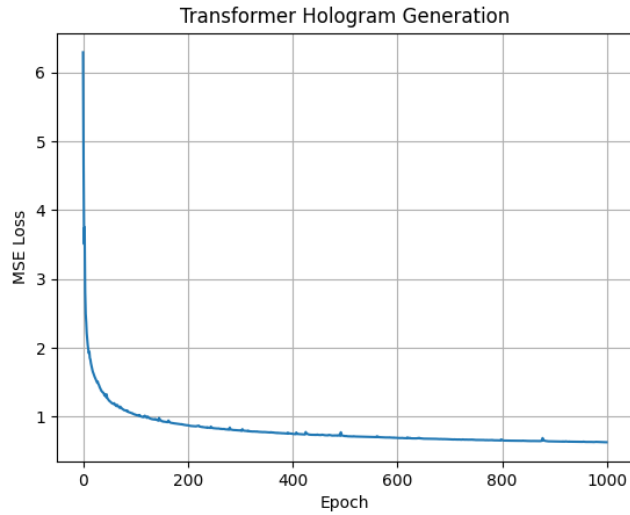


Fig. 2: Training loss (MSE) versus epoch for the final curriculum stage (1000 epochs).

small pixel-level intensity deviations can appear visually exaggerated when magnified; however, at native scale the predicted far-field intensities maintain coherent global structure consistent with the desired patterns. These results support the conclusion that the model learns a transferable inverse diffraction mapping rather than memorizing training exemplars.

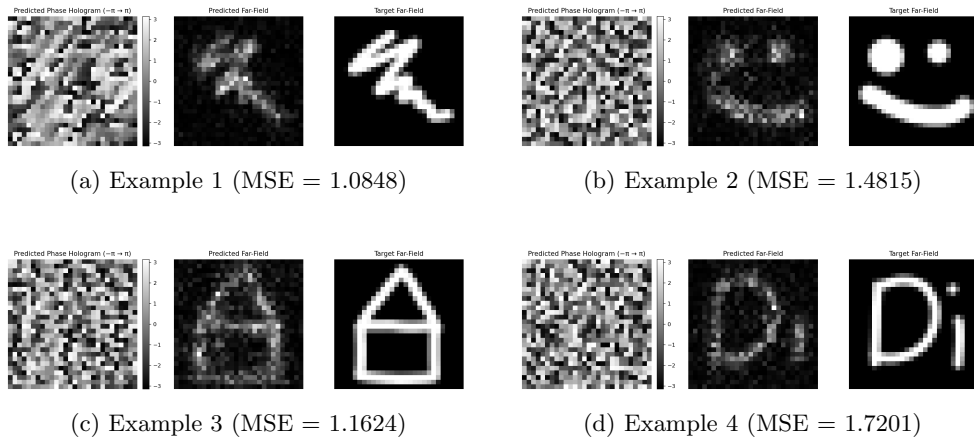


Fig. 3: Generalization to unseen 28×28 custom targets. Each subfigure (a)-(d) corresponds to a different target. Within each subfigure (left to right): predicted phase hologram $[-\pi, \pi]$, predicted far-field intensity, and target intensity.

Table 4: Generalization performance on custom 28×28 targets.

Example	MSE
1	1.0848
2	1.4815
3	1.1624
4	1.7201

3.4 High-Resolution Single-Target Demonstration

While Sections 3.1–3.3 evaluate generalization at low spatial resolution, we next isolate a separate concern: numerical stability and scalability of the physics-in-the-loop formulation at higher resolution.

To test numerical stability at higher spatial resolution, we conducted a separate 500×500 experiment using the same physics-in-the-loop formulation, trained on a single fixed target image (no distribution-level variation). This experiment is intended to demonstrate scalability and stable optimization under exact FFT-based Fraunhofer propagation, rather than high-resolution distribution-level generalization.

Figure 4 shows the optimization trajectory. Starting from an effectively random phase initialization, coarse training yields the emergence of large-scale structure in the far-field reconstruction, while subsequent refinement improves global coherence and reduces residual error under the same phase-only constraint. The final reconstruction achieves substantially lower error than initialization, indicating stable convergence at 500×500 without introducing a learned propagation surrogate.

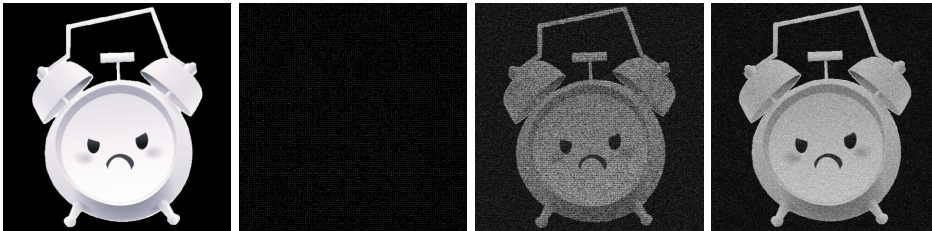


Fig. 4: Optimization progression under coarse-to-refinement training. For each panel (left to right): (a) target intensity, (b) initialization (MSE=8.2567), (c) end of coarse training (MSE=0.4803), and (d) end of refinement (MSE=0.1032). Each image in (b)-(d) shows the predicted far-field from the model’s predicted phase hologram. Progressive emergence of coherent structure demonstrates stable physics-constrained optimization.

4 Discussion and Conclusion

The results demonstrate that transformer-based architectures trained with explicit physics-in-the-loop optimization can stably generate phase-only far-field holograms under exact FFT propagation. Across synthetic patterns, digit subsets, and manually constructed targets, the model converges without collapse and produces coherent reconstructions that preserve global structure. The observed OOD behavior further suggests the network learns aspects of the inverse diffraction mapping rather than merely memorizing training exemplars.

A central observation is the influence of patch size on optimization. Coarse tokenization (patch size 14 for 28×28 inputs) restricts high-frequency phase variation and acts as an implicit regularizer, improving stability and suppressing artifact-like attractors. In contrast, finer tokenization increases spatial degrees of freedom but expands the phase search space and may require curriculum structure or hierarchical refinement. These results indicate patch structure is not merely an implementation detail, but a geometric constraint that shapes the optimization landscape.

The low-resolution regime (28×28) should be interpreted with care: at such resolution, small intensity misplacements can appear disproportionately severe when magnified. The separate 500×500 single-target experiment confirms that the formulation remains numerically stable at substantially higher spatial resolution, supporting scalability of the physics-in-the-loop approach (while not establishing high-resolution generalization).

Generalization is strongly influenced by training diversity. Curriculum training from structured primitives toward more complex targets encourages stable convergence and broader transfer. Increased model capacity and richer training distributions are likely to further improve reconstruction fidelity, particularly when coupled with structured refinement schedules.

Batch size and staged refinement also affect optimization dynamics. Later-stage refinement with smaller batches appears to encourage fine-scale correction without destabilizing previously learned global structure, resembling a multi-scale optimization strategy that may be well suited to diffraction-based inverse problems.

While intensity-domain MSE provides a simple and physically grounded objective, it does not necessarily align with perceptual or structural fidelity in diffraction reconstructions. Future work should explore hybrid objectives that combine energy consistency with structure-aware terms (e.g., frequency-weighted penalties or multi-term losses) to better balance global coherence and fine detail under phase-only constraints.

Future directions include: (1) developing loss functions tailored to phase-only diffraction beyond vanilla MSE, (2) scaling to higher resolutions with distribution-level generalization, and (3) integrating camera-in-the-loop calibration for real optical validation. Ultimately, a full end-to-end pipeline combining learned phase generation, physical propagation, and hardware-aware correction may enable robust, scalable far-field CGH grounded in both physics and data-driven optimization. In experimental settings, the forward optical model may deviate from ideal Fraunhofer propagation due to SLM non-idealities, optical aberrations, and camera response nonlinearities. In such cases, augmenting or replacing the analytical propagation operator with a learned

surrogate model calibrated to hardware measurements may improve reconstruction fidelity while preserving the overall physics-in-the-loop training paradigm.

In summary, this work establishes a proof-of-concept physics-in-the-loop framework for phase-only far-field hologram generation using transformers. Global self-attention is structurally compatible with the nonlocal coupling imposed by Fourier diffraction, enabling stable, fast, single-pass hologram synthesis under exact physical propagation without learned forward surrogates.

Declarations

- Data availability
The MNIST and Fashion-MNIST datasets are publicly available. The other datasets used in this study, including the synthetic targets, will be made available upon publication.
- Code availability
The code used to train and evaluate the proposed model will be made publicly available upon publication.

Selective disclosure (arXiv version)

Certain implementation details will be provided in a journal version.

Author Contributions

Dilawer Singh conceived the original idea. He developed the physics-in-the-loop transformer framework, designed and implemented the full experimental pipeline, conducted all experiments, analyzed the results, and wrote the manuscript. Antoni J. Wojcik contributed through technical discussions and conceptual feedback. Professor Tim D. Wilkinson provided supervisory guidance and contributed to discussions regarding experimental validation and research direction. All authors reviewed and approved the final manuscript.

References

- [1] Goodman, J. W. *Introduction to Fourier Optics* 4 edn (W. H. Freeman, 2017).
- [2] Gerchberg, R. W. & Saxton, W. O. A practical algorithm for the determination of phase from image and diffraction plane pictures. *Optik* **35**, 237–246 (1972).
- [3] Fienup, J. R. Phase retrieval algorithms: A comparison. *Applied Optics* **21**, 2758–2769 (1982).
- [4] Rivenson, Y., Zhang, Y., Günaydn, H., Teng, D. & Ozcan, A. Phase recovery and holographic image reconstruction using deep learning in neural networks. *Light: Science & Applications* **7**, 17141–17141 (2017). URL <https://www.nature.com/articles/lsa2017141>.
- [5] Shimobaba, T. *et al.* Deep-learning computational holography: A review. *Frontiers in Photonics* **Volume 3 - 2022** (2022). URL <https://www.frontiersin.org/journals/photonics/articles/10.3389/fphot.2022.854391>.
- [6] Eybposh, M. H., Caira, N. W., Atisa, M., Chakravarthula, P. & Pégard, N. C. Deepcgh: 3d computer-generated holography using deep learning. *Opt. Express* **28**, 26636–26650 (2020). URL <https://opg.optica.org/oe/abstract.cfm?URI=oe-28-18-26636>.

- [7] Peng, Y., Choi, S., Padmanaban, N. & Wetzstein, G. Neural holography with camera-in-the-loop training. *ACM Trans. Graph.* **39** (2020). URL <https://doi.org/10.1145/3414685.3417802>.
- [8] Chakravarthula, P., Tseng, E., Srivastava, T., Fuchs, H. & Heide, F. Learned hardware-in-the-loop phase retrieval for holographic near-eye displays. *ACM Trans. Graph.* **39** (2020). URL <https://doi.org/10.1145/3414685.3417846>.
- [9] Kangsheng, S. *et al.* Fast generation algorithm of high-quality holograms based on attention convolutional neural network. *Acta Physica Sinica* **74**, 084203–1–084203–10 (2025). URL <https://wulixb.iphy.ac.cn/en/article/doi/10.7498/aps.74.20241713>.
- [10] Singh, D., Wojcik, A., Gardner, S. & Wilkinson, T. D. Fully-complex hologram recognition using neural networks. *SPIE Proceedings* **13719**, 331–342 (2025).
- [11] LeCun, Y., Bottou, L., Bengio, Y. & Haffner, P. Gradient-based learning applied to document recognition. *Proceedings of the IEEE* **86**, 2278–2324 (1998).
- [12] Vaswani, A. *et al.* Attention is all you need. *CoRR* **abs/1706.03762** (2017). URL <http://arxiv.org/abs/1706.03762>.
- [13] Dosovitskiy, A. *et al.* An image is worth 16x16 words: Transformers for image recognition at scale. *CoRR* **abs/2010.11929** (2020). URL <https://arxiv.org/abs/2010.11929>.
- [14] LeCun, Y., Cortes, C. & Burges, C. J. C. The mnist database of handwritten digits. <http://yann.lecun.com/exdb/mnist/>. Accessed 2025-09-18.
- [15] Xiao, H., Rasul, K. & Vollgraf, R. Fashion-mnist: A novel image dataset for benchmarking machine learning algorithms. *arXiv preprint arXiv:1708.07747* (2017). URL <https://arxiv.org/abs/1708.07747>.